Sittakul, V., & Cryan, MJ. (2007). A fully bidirectional 2.4-GHz Wireless-Over-Fiber system using Photonic Active Integrated Antennas (PhAIAs). *Journal of Lightwave Technology*, *25*(11), 3358 - 3365. https://doi.org/10.1109/JLT.2007.909199

A Fully Bidirectional 2.4-GHz Wireless-Over-Fiber System Using Photonic Active Integrated Antennas (PhAIAs)

Vitawat Sittakul and Martin J. Cryan, *Senior Member, IEEE*

***Abstract*—This paper describes a low-cost scheme for implementing in-building distributed antenna systems using the photonic-active-integrated-antenna (PhAIA) concept, whereby photonic devices are integrated directly with planar antennas. Deembedded input impedance is measured for an 850-nm vertical-cavity surface-emitting laser and photodiode from 0–10 GHz, and the devices are matched directly to the nonradiating edge of a rectangular-microstrip-patch antenna. Link gain, 1-dB compression point, and spurious-free dynamic range are measured in the links. The fully bidirectional system, which is far from being completely optimized, is then tested over a 300-m laboratory-based multimode fiber link and a 220-m in-building dark-fiber link. Results are shown for throughput and signal-to-noise ratio, and this paper shows that such systems can achieve up to 10-m RF range, at reduced throughput, with no RF amplification.**

***Index Terms*—Antennas, photodiodes, radio-over-fiber, VCSELs.**

I. Introduction

THE photonic-active-integrated-antenna (PhAIA) concept is the intimate integration of photonic devices with antennas [1]; it is an extension to the well-known active-integrated-antenna (AIA) concept from the microwave-engineering field [2]. The fact that the photonic device and antenna are highly integrated means that very efficient impedance matching can be achieved, which can lead to improved link gain [3]. It could also lead to much reduced packaging and fabrication costs. These ideas can be extended to full monolithic integration, and some work has been done on photodiode (PD)–antenna integration [4]; however, this has yet to be extended to laser–antenna integration.

There is much current interest in low-cost wireless-over-fiber (WoF) systems [5]–[7] for distribution of mobile-phone and WiFi signals within buildings. In applications such as this, cost will be critical, and the improved link gain and reduced packaging costs that can be achieved with PhAIAs could play an important role.

This paper presents results for a full-duplex WoF system using vertical-cavity surface-emitting lasers (VCSELs) and PDs integrated with microstrip-patch antennas. A schematic of the link is shown in Fig. 1. Here, a universal-serial-bus (USB) wireless adapter operating in 802.11b mode is used as an access point; this is connected via a coax splitter to a VCSEL transmitter and a PD receiver. Two types of fiber link are then assessed: first, a laboratory-based 300-m MMF link, and second, a 220-m in-building dark-fiber MMF link. In both cases, the fibers are connected to a VCSEL–antenna and a PD–antenna, and a wireless-enabled laptop is then placed a distance from the PhAIAs. This configuration could form the basis for a range-extension system, which would tap RF power from an existing access point and feed this into an in-building fiber network and retransmit the access-point signal from the low-cost PhAIA-based remote node. It should be noted here that no RF amplification is being used—this will be important for maintaining low-cost operation and is particularly important at the remote node. It may even be possible to power the remote node using power-over-fiber techniques, and the low operating current of the return VCSEL will ideally be suited to this application.

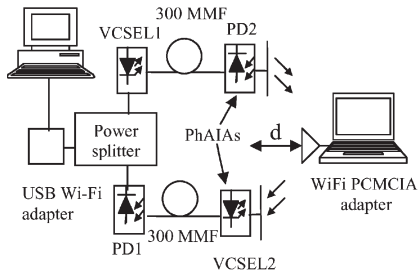

Fig. 1. System configuration.

In Section II of this paper, the performance of individual components of the link are measured and this leads on to link gain and linearity characterization in Section III. Section IV assesses the performance of the VCSEL–antennas and PD–antennas, and Section V assesses the complete link in terms of throughput and signal-to-noise ratio (SNR). Finally, Section VI gives the conclusions and future direction for this work.

II. Individual-Component Performance

A. VCSELs

The link is comprised of two low-cost 850-nm VCSELs from Truelight (www.truelight.com.tw). In order to study the tradeoffs between threshold current, slope efficiency, and output

Manuscript received February 15, 2007; revised September 19, 2007. The work of V. Sittakul was supported by Ph.D. funding through a Royal Thai Government Scholarship.

The authors are with the Photonics Research Group, Department of Electrical and Electrical Engineering, University of Bristol, BS8 1TR Bristol, U.K. (e-mail: m.cryan@bristol.ac.uk).

Digital Object Identifier 10.1109/JLT.2007.909199

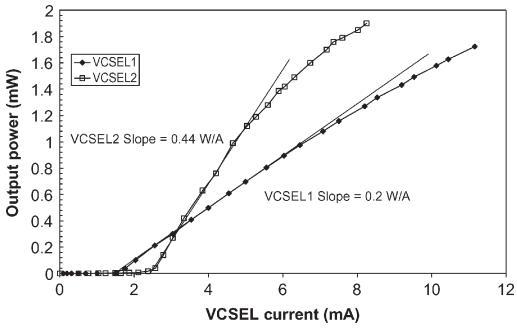

Fig. 2. *L–I* curves for VCSEL 1 and VCSEL 2.

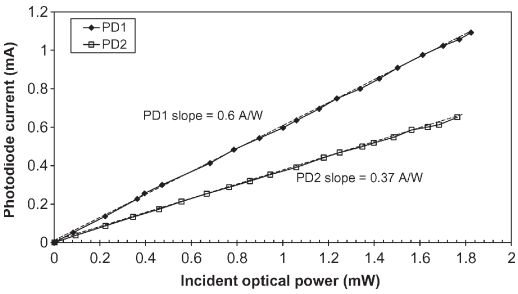

Fig. 3. Photocurrent versus incident optical power for PD1 and PD2.

power, different VCSELs are currently being used within the link. At the access-point end, a standard VCSEL (VCSEL 1: TSD-8B12-000) with medium slope efficiency is being used, whereas the remote end employs a high-slope-efficiency device (VCSEL 2: TSD-8B12-017). Lower threshold-current devices are also under investigation and will be the subject of future work. Fig. 2 shows *L–I* curves for VCSEL 1 and VCSEL 2; these are measured by coupling power directly into a cleaved MMF. It is shown that VCSEL 2 gives superior performance with a slope efficiency of 0.44 W/A, as compared to 0.2 W/A for VCSEL 1.

B. Photodiodes

Two low-cost 850-nm PDs are used in the link; in this case, only one type of device is used: a GaAs PIN from Truelight (TPD-8D12-006). The most important parameter of a PD is its responsivity. To measure the responsivity of the PDs, the incident optical power generated from VCSEL 1 with bias current varying from 0 to 10 mA was fed into the PD via a 1-m length MMF with a flat-cleaved facet. The PD current was plotted as a function of incident optical power. The results for PD1 and PD2 are shown in Fig. 3. The slope of the graph shows the responsivity of PD1 to be 0.6 A/W and PD2 to be 0.37 A/W. This variation is most likely due to the sensitivity to alignment between the PD and the MMF.

C. Input Impedance of VCSELs and PDs

The key feature of a PhAIA-based system is the ability to achieve relatively wideband conjugate matching between the photonic device and the antenna with no, or at least very simple, matching networks. This results in maximum power transfer and can result in significant improvement in link gain

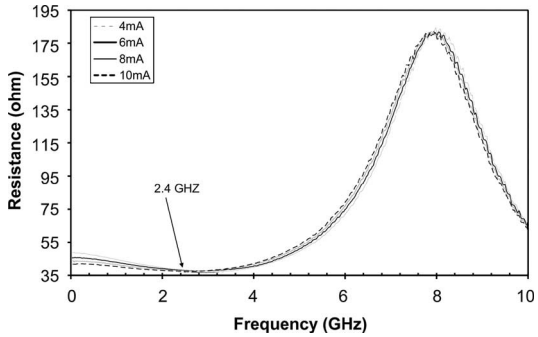

Fig. 4. VCSEL-2 deembedded input resistance versus frequency for different VCSEL bias currents.

over a narrow bandwidth [3]. This makes the approach ideally suited to WiFi-signal-distribution applications, and multiband or wideband antennas can be used to distribute signals simultaneously in other bands, such as 1.8 and 5.2 GHz. To achieve conjugate matching, it is required to have a detailed knowledge of the input impedance of the photonic device. However, this has not been widely studied, since in standard optical-communication systems, simple wideband-matching techniques, such as series resistors, are often used and detailed knowledge of the input impedance is less critical. However, since WoF systems are often narrowband, very efficient conjugate matching can be achieved through the use of lossless-matching networks or, in the case of PhAIAs, by positioning the contact point of the photonic device to the antenna at the appropriate position to achieve matching. This is due to the fact that the widely varying input impedances can be obtained from planar antennas, from very low to 200–300 Ω. To this end, the input impedance of both the VCSEL and PD are presented here. PD impedances were presented in [1], but this was for a 1550-nm device. In addition, 850-nm VCSEL return loss was shown; however, it is believed that this paper is one of the first to present detailed studies of deembedded VCSEL and PD input impedance in the 0–10-GHz frequency range. The term deembedding refers to the ability of a vector network analyzer, used to measure the impedance, to move its reference plane, such that the phase shift introduced by connectors and microstrip transmission lines can be removed. This leads to an accurate measurement of input impedance, and the results are shown in Figs. 4–7. The simple approach taken here assumes that the effect of discontinuities and non-50-Ω transmission lines is negligible, which is reasonable at 2.4 GHz, but the accuracy will reduce toward 10 GHz. The VCSEL and PD are both mounted on microstrip carriers, which include bond wires and ground connections; thus, any impedance measurement will also include these parasitic effects. Care has been taken to reduce these effects to a minimum.

Figs. 4 and 5 show that the VCSEL input impedance is close to $37 + j2\ \Omega$ for frequencies close to 2.4 GHz and at typical bias currents. This implies that quite-straightforward conjugate matching can be achieved, since the reactive part of the impedance is very low. Figs. 6 and 7 show the resistance and reactance for the PD, and as might be expected, it is much more capacitive in nature with an impedance at 2.4 GHz of $10 - j100\ \Omega$. This is a zero-biased value, which would become

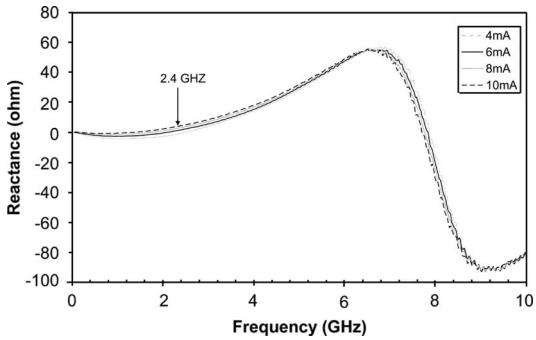

Fig. 5. VCSEL-2 deembedded input reactance versus frequency for different VCSEL bias currents.

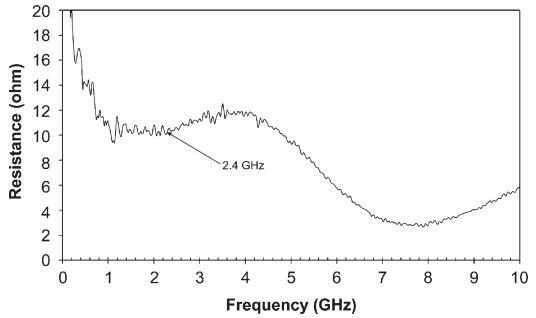

Fig. 6. PD-1 resistance versus frequency.

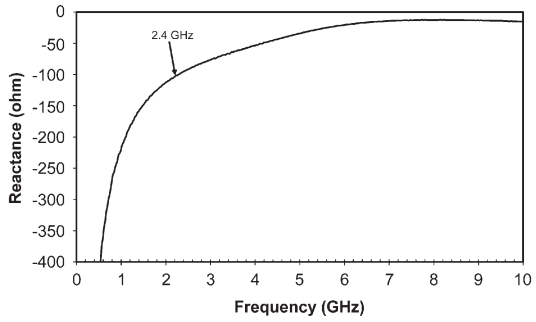

Fig. 7. PD-1 reactance versus frequency.

less capacitive as reverse bias is applied; however, all results in this paper are at zero-bias level. This implies that conjugate matching will be more difficult and would require additional series or parallel matching elements to be added. This more complex matching has not been implemented here, and the PD has been placed close to the 10-Ω input impedance point on the antenna. This is close to the center of the nonradiating edge of the antenna—where very low input impedances are found [8].

III. Basic Link Gain

This section brings together the individual components into a WoF system and characterizes its basic operation in terms of gain and linearity before integrating the components with planar antennas. Fig. 8 shows the measurement setup. The bias tee connected to the PD enables the photocurrent to flow from the PD—an important requirement in obtaining wideband operation.

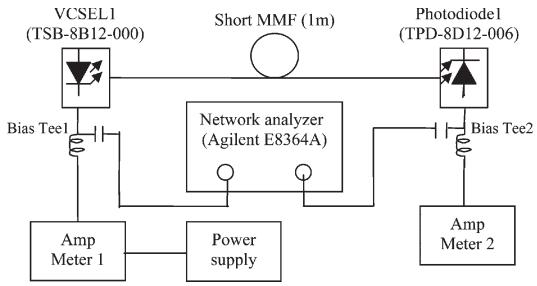

Fig. 8. Diagram of the basic-link gain measurement.

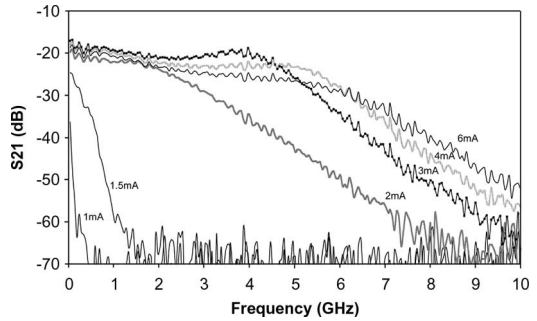

Fig. 9. S_{21} versus frequency at different VCSEL-1 bias currents.

Fig. 9 shows the measured results for different VCSEL bias currents. It is shown, as expected, that the bandwidth increases for increasing forward bias; however, this can be at the expense of noise and linearity performance. The linearity of the link will be studied in subsequent sections. The main point to draw from the graph is that the chosen VCSEL and PD have sufficient bandwidth for operation at 2.4 GHz and would be useable up to 5–6 GHz, depending on system-performance specifications.

It is useful to take the individual-component characteristics obtained in Section II and see if the low-frequency behavior of the link can be predicted. It is well known that the low-frequency link gain can be described by the following relationship [3]:

$$G = S_{\rm l}^2 \eta_{\rm lf}^2 T_{\rm f}^2 \eta_{\rm fd}^2 S_{\rm d}^2 \tag{1}$$

where $S_{\rm l}$ is the slope efficiency of the laser, $S_{\rm d}$ is the responsivity of the PD, $\eta_{\rm lf}$ and $\eta_{\rm fd}$ are the coupling efficiencies from the laser and PD to MMF, respectively, and $T_{\rm f}$ is the loss in the fiber. This assumes identical resistive source and load impedances in the system.

Since the slope efficiencies are measured directly into the MMF, they can be grouped together with the coupling-efficiency terms, and the loss of the short length of MMF can be ignored. Taking a VCSEL-1 slope efficiency of 0.2 and a PD responsivity of 0.6, a link gain is then obtained of -18.41 dB, close to the low-frequency value shown in Fig. 9.

From the data in Fig. 9, we can also evaluate the optimum VCSEL bias current for maximum link gain. Fig. 10 shows results for this at 2.4 GHz. It is shown that optimum link gain is found at a value of 3 mA. It will be shown later that this is not the same optimum in terms of linearity, and thus, a tradeoff will need to be made between these various factors.

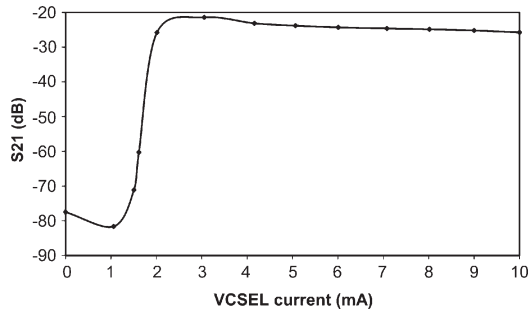

Fig. 10. S_{21} at different VCSEL-1 bias currents at 2.4 GHz.

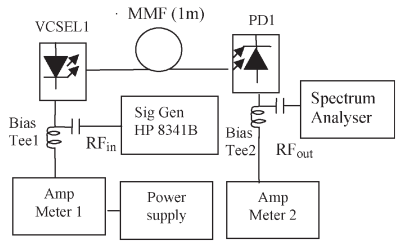

Fig. 11. Measurement of 1-dB gain-compression point of the basic link.

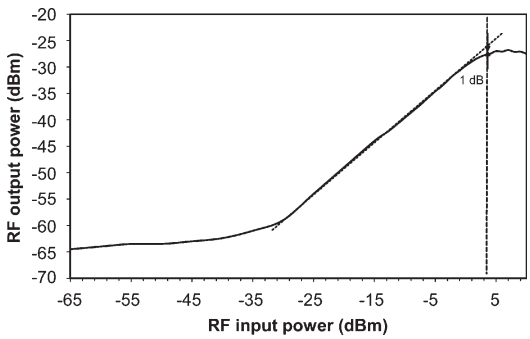

Fig. 12. RF output power as a function of RF input power, bias current = 8 mA, modulation frequency = 2.4 GHz, and fiber length = 1 m.

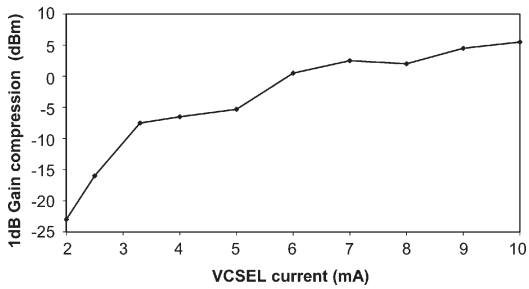

Fig. 13. VCSEL-1 current versus 1-dB gain-compression point referred to the input.

A. Linearity of the Basic Link

In any communications system, linearity is a critical factor. The linearity of VCSEL-based radio-over-fiber (RoF) links has been studied before [9], but it is important to assess the performance of the specific devices being used here. To this end, both 1-dB compression point $(G_{1\,\mathrm{dB}})$ and spurious-free dynamic range (SFDR) have been measured and are presented in the following sections.

1) Basic-Link 1-dB Gain Compression: All active RF devices are ultimately nonlinear in operation. When driven with a large-enough RF signal, gain compression will occur; this is characterized by the 1-dB gain-compression point. Using the setup shown in Fig. 11, the 1-dB gain compression of the basic link was measured for different VCSEL-1 bias currents at the modulation frequency of 2.4 GHz.

In this paper, the RF input signal from a signal generator (HP8341B) was fed to VCSEL 1 together with the bias current through the bias tee. The RF output power from the PD is monitored by the spectrum analyzer and plotted versus the RF input power. This is shown in Fig. 12 for a certain bias current (8 mA) and modulation frequency (2.4 GHz) using a 1 m of 62.5/125-μm MMF. It should be noted that the link gain can be derived from this data, and it is shown to be slightly worse than when it was measured directly using the vector network analyzer (VNA). This is due to the extra cables used in the gain-compression measurement and slight differences in MMF alignment between the two measurements. Fig. 13 summarizes the measured 1-dB gain compression at different VCSEL-1 bias currents at a modulation frequency of 2.4 GHz.

Fig. 13 shows that the 1-dB gain-compression point is increasing with increasing VCSEL bias and has a maximum value of +5 dBm at 10-mA VCSEL bias. It is shown that the optimum point has not been reached; however, as will be seen later, in terms of overall system performance, the optimum has been found to be within the above range.

2) SFDR of the Basic Link: In Section III, the linear gain of the basic link was measured. The gain was derived from the RF power at the fundamental frequency. However, because of the nonlinearity of the VCSEL and PD, the RF output power will contain not only the signal at the fundamental frequency but also at harmonic frequencies. SFDR is a measure of the performance of a nonlinear system when operating with more than one input signal. Here, a two-tone measurement will be performed. SFDR can mathematically be defined as the following [10]:

$$\mathrm{SFDR_{dB}} = 2/3(P_{3\mathrm{I}} - N_{\mathrm{l}})\ [\mathrm{dB \cdot Hz^{2/3}}] \tag{2}$$

where $P_{3\mathrm{I}}$ is the third-order intercept point in (dBm), and N_{l} is the noise floor of the link in (dBm/Hz).

SFDR performance has been studied previously [11], and again, the performance of the devices being used here needs to be confirmed. Fig. 14 shows the measurement setup used to perform the tests.

To investigate the SFDR of the link, a two-tone measurement was performed using MMF and VCSEL 1 as the light source. Two equal output signals separated by 1 MHz from the signal generator and the network analyzer at $f_1 = 2.4$ and $f_2 = 2.401$ GHz are fed in the VCSEL 1. This results in output signals at $f_1 = 2.4$, $f_2 = 2.401$, $2f_1 - f_2 = 2.399$, and $2f_2 - f_1 = 2.402$ GHz. As can be seen from (2), as well as the third-order intercept point $P_{3\mathrm{I}}$, the noise floor of the link N_{l} is also required in order to calculate the SFDR. The noise floor of the spectrum analyzer is limited to -85 dBm in a 1-kHz

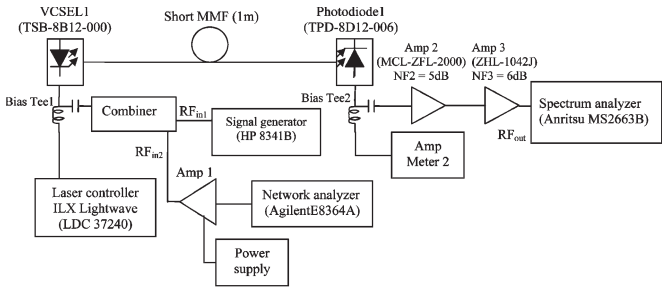

Fig. 14. Measurement of SFDR of VCSEL 1.

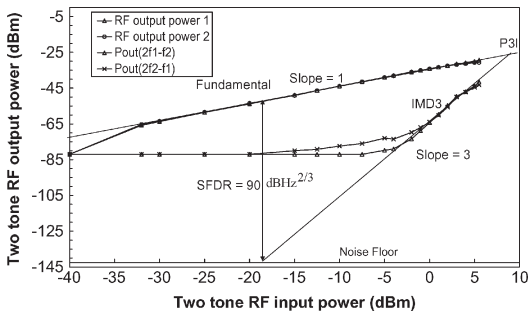

Fig. 15. Two-tone RF input versus RF output at VCSEL-1 current of 7 mA.

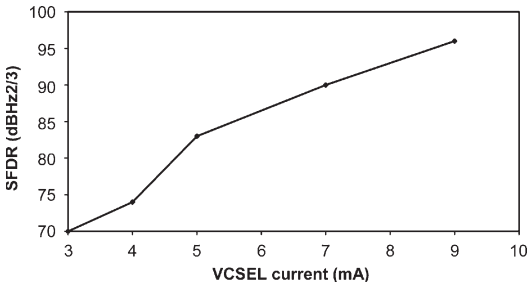

Fig. 16. SFDR versus VCSEL-1 current.

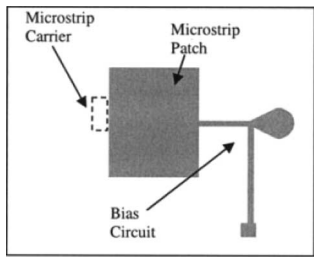

Fig. 17. Front view of PhAIA showing layout of microstrip patch, bias network, and photonic device carrier mounted on the reverse side.

bandwidth; however, the link noise is below this level. This problem can be solved by using the two amplifiers Amp 2 and Amp 3 with gains of 17.48 and 16.2 dB, respectively. This raises the measured-link noise floor above that of the spectrum analyzer [11].

The noise floor of the basic link will be amplified by the Amp 2 and Amp 3 with total gain of 33.68 dB and total noise figure $\mathrm{NF_T}$ of 5.1 dB found from the well-known relationship for the noise figure of a cascade of amplifiers. The measured value of the noise floor is now found to be -73.7 dBm, which is above the noise floor of the spectrum analyzer. Therefore, the intrinsic noise floor of the basic link can be calculated to be $-73.7 - 33.68 - 5.1 = -112.48$ dBm in a bandwidth of 1 kHz and converted to -142.48 dBm in a bandwidth of 1 Hz. It has been assumed that the spectrum-analyzer filter has an ideal rectangular shape for this calculation, whereas in reality, it will be close to Gaussian and this will introduce a slight approximation. In order to confirm that the estimate of the noise floor is reasonable, we can calculate a value directly from knowledge of various parameters within the link. The main sources of noise within links such as this are thermal noise, shot noise, and relative intensity noise (RIN). This link is found to be dominated by RIN, and (3) shows how the noise power at the output of the PD can be calculated [3]

$$\frac{\langle I_{\mathrm{d}}\rangle^2}{2} 10^{\frac{\mathrm{RIN}}{10}} R_L \tag{3}$$

where I_{d} is the average PD current, and R_L is the PD load resistance, assumed to be 50 Ω. Assuming a responsivity for the PD of 0.6 A/W, an average optical power of 1 mW, and a RIN value of -130 dB/Hz [14], which is a typical value for these types of lasers, we obtain a noise power of -150.5 dBm/Hz. Bearing in mind the assumptions that have been made, this is in reasonable agreement with the measured value.

The amplifier Amp 1 is used to boost the output signal of the network analyzer from 0 dBm up to 5.5 dBm, and the signals from the network analyzer and the signal generator were combined and fed to the VCSEL. The power of the fundamental and third-order intermodulation products are plotted against the RF input power, as shown in Fig. 15.

The SFDR was extracted from the data shown in Fig. 15 at different VCSEL-1 bias currents and is shown in Fig. 16.

The results show that there is an increase in SFDR with increasing VCSEL-1 current. The SFDR can be improved from 70 to 96 dB $\cdot$ $\mathrm{Hz}^{2/3}$ by increasing the VCSEL-1 bias current from 3 to 9 mA. It is shown that the noise floor is an important factor in improving the SFDR, and optimization of the link with respect to noise performance will be carried out in future systems. The SFDR obtained in this paper satisfies the requirements for a number of applications, such as microcellular personal-communication systems and WLAN [12], [13]. The SFDR obtained here is close to that obtained in [11], although the effects of fiber length have not been investigated here.

IV. Photonic Active Integrated Antennas (PhAIAs)

Having assessed the individual components and the basic link, the PhAIAs can now be studied in detail. Fig. 17 shows a front view of the planar-microstrip antenna being used.

The antenna is a standard rectangular microstrip patch designed to operate at 2.4 GHz. A transmission-line biasing circuit is also used so that VCSEL bias or PD current can flow across the patch—further reducing component count. A microstrip carrier is used to mount the photonic device and is soldered on to the reverse side of the antenna, creating a uniform ground plane for both antenna and microstrip carrier. Fig. 18(a) and (b) show side views of the VCSEL- and PD-integrated antenna devices. It is shown that current can flow

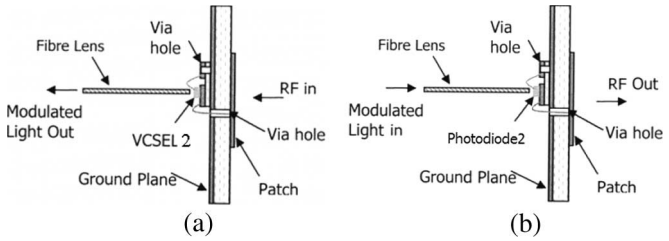

Fig. 18. Configuration of PhAIAs. (a) VCSEL 2. (b) PD 2.

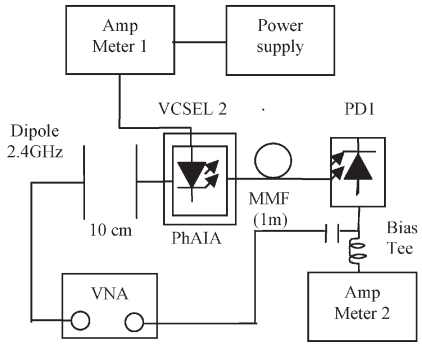

Fig. 19. S_{21} measurement diagram of VCSEL–PhAIA.

across the antenna, through the bond wire onto the microstrip carrier, through the VCSEL, and back to the common ground through a second bond wire and ground via.

The VCSEL and PD are connected close to the center of the nonradiating edge of the antenna; this will be close to the 10–40 Ω required for matching the real parts of the impedances. In the case of the PD, further matching will be required to obtain a finally optimized system.

A. Frequency Response of a VCSEL–PhAIA

The system link gain using a VCSEL–PhAIA can now be assessed, and Fig. 19 shows the configuration. The key feature here is that, now, a dipole antenna is required to radiate RF power onto the device. The dipole is a simple wire dipole designed to operate at 2.4 GHz. The arrangement is identical to that shown in Fig. 8, but now, there is a wireless link within the setup; in this case, a short distance of 10 cm has been used. The measured link gain is shown in Fig. 20.

The most obvious feature in Fig. 20 is the strong resonant response around 2.4 GHz; this is produced by resonant nature of the patch antenna; the dipole response will also contribute to this—but this will tend to be a wider band. The figure also shows a reduction of around 28 dB as compared to the basic-link results shown in Fig. 9. This is due to a number of factors: First, a free-space loss will be introduced between the antennas. Second, there will be mismatch loss at both the dipole antenna and between the VCSEL and patch antenna; future systems will have this reduced to a minimum. Finally, the fiber alignment in this case can be more difficult since the VCSEL is mounted on a flexible antenna substrate. A fully portable system will be discussed later in this paper where this fiber-alignment problem has been addressed. The peaks observed around 0.8 and 1.4 GHz are due to radiation from the bias circuit, and that

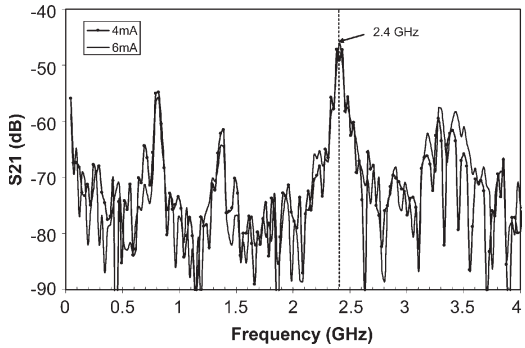

Fig. 20. VCSEL–antenna S_{21} versus frequency with different VCSEL-2 bias currents.

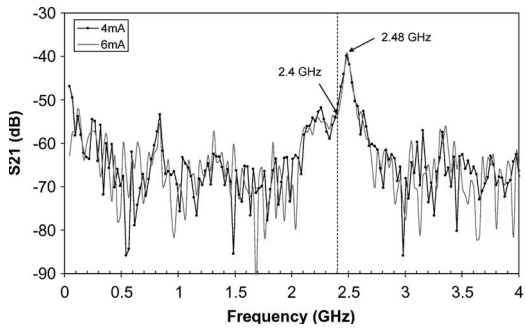

Fig. 21. PD–antenna S_{21} versus frequency at VCSEL-1 current of 2.48 mA.

around 3.3 GHz is the other polarization of the patch antenna being observed at a lower level.

This measurement configuration will enable the optimization of VCSEL position on the antenna to give conjugate matching and, hence, maximum link gain. However, as will be shown, even this unoptimized configuration can give good overall system performance.

B. Frequency Response of PD–PhAIA

A similar test setup is used to show the PD–antenna performance, and the results are shown in Fig. 21.

Here, again, the resonant response of the patch antenna is clearly observed; however, in this case, it is shown that the frequency is offset from 2.4 GHz. This is caused partly by antenna-fabrication tolerance but also by the loading effect the PD has on the antenna. In future iterations of this system, the loading effects of both VCSEL and PD will be incorporated into the design cycle. Thus, within the current system, there is ∼10-dB link loss being introduced by the frequency offset of the PD–antenna, implying that future systems will have much better overall performance. The other point to note here is that the bandwidth of the system is quite narrow. This is due to the fact that a high-dielectric-constant substrate has been used with $\varepsilon_r = 10.2$. This reduces the size of the antenna but also reduces the bandwidth; future systems will use very-low-cost substrates on FR4 material, which has a much lower $\varepsilon_r = 4.5$ and, thus, a wider bandwidth.

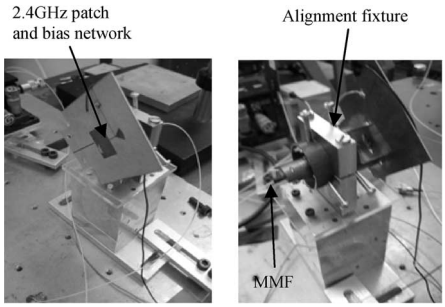

Fig. 22. Portable PhAIA with PD. (Left) Front view. (Right) Back view.

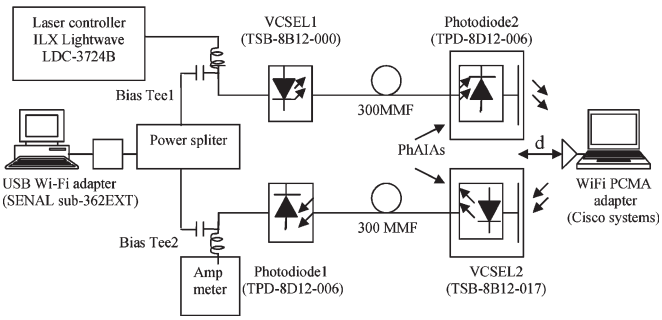

Fig. 23. Diagram of bidirectional link.

V. Experimental Setup for Bidirectional Link Using PhAIAs

One of the difficulties of working with both photonic and antenna devices is that optical tables are normally required for the photonic devices, and these large metal objects can severely effect radiation patterns and antenna performance. Thus, a low-cost mount has been developed, as shown in Fig. 22, which allows accurate alignment of the MMF to the optical device but does not require $x-y-z$ stages to be used. This will enable these devices to be characterized within anechoic chambers, as is required for any WiFi device.

All the components discussed in the preceding sections are now brought together in a fully bidirectional twin-fiber-based system. The layout for the system is shown in Fig. 23. A USB wireless adapter was used to mimic a hot-spot, and the external antenna was removed so that the signal could be fed directly into a non-antenna VCSEL and PD transceiver. This system then takes this WiFi signal and can retransmit it using a remote PhAIA-based transceiver after some length of MMF.

There are three main differences between this configuration and that shown in [1]. First, this is fully low cost using two 850-nm VCSELs and two PDs. Second, there is no RF amplification used here—an important point for any low-cost low-dc power system. Finally, only one antenna–antenna link is used. This has the effect of increasing the input power to the link, and this is the main reason why amplification can be removed and why the RF range has increased so dramatically from 10 cm in [1] to around 10 m in this paper. It is felt that this is a commercially viable configuration where RF power can be tapped off coaxially from an existing access point and fed into a purely coaxial transceiver.

At the laptop side, the distance between the PhAIA and the wireless Personal Computer Memory Card International Association (PCMCIA) adapter d was varied from 0.1 to 10 m, and the results for throughput and SNR are shown in Figs. 24 and 25, respectively. The Aironet client utility provided with the Cisco Wireless PCMCIA adapter was used to measure the SNR, and proprietary software provided by Provision Communications (www.provision-comm.com), which is a spin-out from the University of Bristol, was used to measure the throughput of the link. It was found that a WiFi link could be maintained up to a distance of 10 m, and results are presented at different VCSEL-1 bias currents. In this case, VCSEL-2 bias currents are fixed at 4 mA. Fig. 24 shows that the throughput can be higher than 1 MB/s in the range of up to 1.8 m. It is shown that the throughput cannot be measured for VCSEL bias currents of 4 and 6 mA beyond a distance of 5.5 and 6.5 m, respectively. However, by increasing the VCSEL bias current to 8 mA, it is shown that throughput measurements can be extended to 10 m. If the bias current is further increased, the achievable range is reduced; this is most likely due to signal distortion being induced by the nonlinearities of the link. Fig. 25 shows that reasonable SNR can be maintained to 10 m. The setup was then used to stream video across the link, and high-quality video transmission was achieved to a range of 10 m.

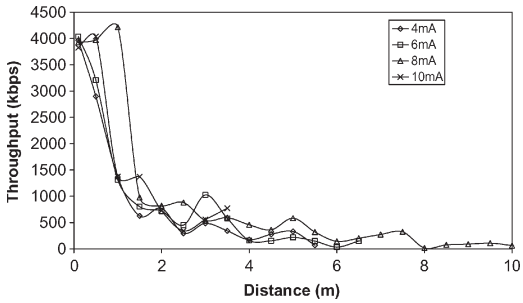

Fig. 24. Throughput versus distance at different VCSEL-1 bias current.

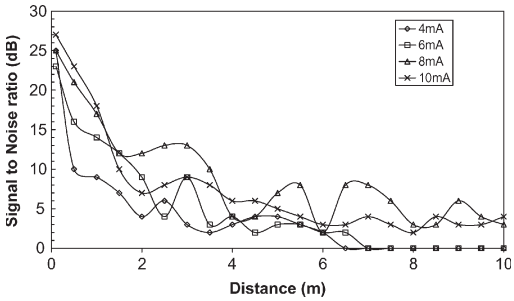

Fig. 25. SNR versus distance at different VCSEL-1 bias current.

These results show that a VCSEL-1 bias current of 8 mA appears to give the best link performance; this value makes a balance between link gain, linearity, and noise performance. It should be noted that no optimization of the VCSEL-2 bias has been performed and that reverse bias can easily be applied to the PDs to further improve this performance. The periodic nature of the results, with respect to distance, are most likely due to multipath-fading effects due the laboratory-based environment in which these results were taken. The portable fixtures shown in Fig. 22 will now enable trials to take place within departmental anechoic-chamber facilities.

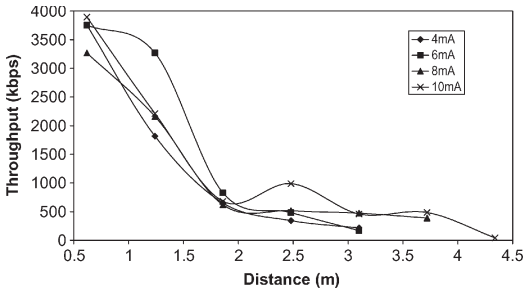

Fig. 26. Throughput versus distance at different VCSEL-1 bias current.

As a further test for the system, trials using in-building dark fiber have taken place over link lengths of 220 m. Results for throughput are shown in Fig. 26.

Reduced-RF-range performance was obtained here due to the fact that the RF loss of the in-building link was greater that the 300-m link, even though it was shorter. This is believed to be due to bending losses within the in-building link.

VI. Conclusion

This paper has presented a detailed study of WoF links based on the PhAIA concept, where photonic devices are integrated directly with planar antennas. This approach will enable very efficient conjugate matching between the photonic device and the antenna to be achieved, which will, in turn, result in improved link gain. The systems described have yet to be optimized in terms of impedance matching, bias currents, and antenna-resonant frequency and bandwidth; thus, much improved performance is expected for future system iterations. The system is inherently very low cost and does not use any RF amplification, although the additions of low-noise amplifiers would be a straightforward extension. This would, however, require substantial dc power at the remote node, and it is felt that this will severely impact the commercial viability of the approach.

Acknowledgment

The authors would like to thank Prof. D. Bull of Provision Communications and P. Ferre for providing the throughput-measurement codes.

References

[1] M. J. Cryan, M. Dragas, J. Kung, V. Jain, F. Fornetti, T. Houle, R. Varrazza, and M. Hill, "A 2.4 GHz wireless-over-fibre transceiver using photonic active integrated antennas (PhAIAs)," *Microw. Opt. Technol. Lett.*, vol. 48, no. 2, pp. 233–237, Feb. 2006.

[2] M. J. Cryan, P. S. Hall, K. S. H. Tsang, and J. Sha, "Integrated active antenna with full duplex operation," *IEEE Trans. Microw. Theory Tech.*, vol. 45, no. 10, pp. 1742–1748, Oct. 1997.

[3] C. H. Cox, III, *Analog Optical Links: Theory and Practice*. Cambridge, U.K.: Cambridge Univ. Press, 2002.

[4] H. Ito *et al.*, "Photonic millimetre-wave emission at 300 GHz using an antenna-integrated uni-travelling-carrier photodiode," *Electron. Lett.*, vol. 38, no. 17, pp. 989–990, Aug. 2002.

[5] A. Das *et al.*, "Design of low-cost multimode fiber-fed indoor wireless networks," *IEEE Trans. Microw. Theory Tech.*, vol. 54, no. 8, pp. 3426–3432, Aug. 2006.

[6] A. Nkansah *et al.*, "Simultaneous dual band transmission over multimode fiber-fed indoor wireless network," *IEEE Microw. Wireless Compon. Lett.*, vol. 16, no. 11, pp. 627–629, Nov. 2006.

[7] C. P. Liu, A. J. Seeds, J. S. Chadha, P. N. Stavrinou, G. Parry, M. Whitehead, A. Krysa, and J. S. Roberts, "Design, fabrication and characterisation of normal-incidence 1.56 μm multiple-quantum-well asymmetric Fabry–Perot modulators for passive picocells," *IEICE Trans. Electron.*, vol. E85-C, no. 1, Jan. 2002.

[8] J. R. James, P. S. Hall, and C. Wood, *Microstrip Antenna Theory and Design*. Stevenage, U.K.: Peregrinus, 1981.

[9] R. E. Schuh, A. Alping, and E. Sundberg, "Penalty-free GSM-1800 and WCDMA radio-over-fibre transmission using multimode fibre and 850 nm VCSEL," *Electron. Lett.*, vol. 39, no. 6, pp. 512–514, Mar. 20, 2003.

[10] W. S. C. Chang, *RF Photonic Technology in Optical Fiber Links*. Cambridge, U.K.: Cambridge Univ. Press, 2002.

[11] C. Carlsson, H. Martinsson, and A. Larsson, "High performance microwave link using a multimode VCSEL and a high-bandwidth multimode fiber," in *Int. Top. Meeting MW, Tech. Dig.*, 2001, pp. 81–84.

[12] J. C. Fan, C. L. Lu, and L. G. Kazovsky, "Dynamic range requirements for microcellular personal communication systems using analog fiber-optic links," *IEEE Trans. Microw. Theory Tech.*, vol. 45, no. 8, pp. 1390–1397, Aug. 1997.

[13] D. M. Cutrer, J. B. Georges, T. H. Le, and K. Y. Lau, "Dynamic range requirements for optical transmitters in fiber-fed microcellular networks," *IEEE Photon. Technol. Lett.*, vol. 7, no. 5, pp. 564–566, May 1995.

[14] W. Mann and K. Petermann, "VCSEL-based miniaturised E-field probe with high sensitivity and optical power supply," *Electron. Lett.*, vol. 38, no. 10, pp. 455–456, May 9, 2002.

Vitawat Sittakul was born in Bangkok, Thailand, in March 1979. He received the B.Eng. degree in telecommunication from Chulalongkorn University, Bangkok, Thailand, in 2000 and the M.Sc. degree (with distinction) in optical and communication systems from Northumbria University, Newcastle, U.K., in 2003. He has been working toward the Ph.D. degree with the Department of Electrical and Electronic Engineering, University of Bristol, Bristol, U.K., since 2006.

From 2003 to 2004, he was a Measurement Engineer with Fabinet, where he was a global engineering- and manufacturing-services provider. From 2004 to 2006, he was a Senior RF Engineer with Advance Information Service Company, Ltd., which is the biggest mobile-service provider in Bangkok. His research interest is in radio-over-fiber.

Martin J. Cryan (S'91–M'95–SM'01) received the B.Eng. degree in electronic engineering from the University of Leeds, Leeds, U.K., in 1986 and the Ph.D. degree from the University of Bath, Bath, U.K., in 1995.

He worked in the industry for five years as a Microwave Design Engineer. From 1994 to 1997, he was a Researcher with the University of Birmingham, Birmingham, U.K., where he worked on active integrated antennas. From 1997 to 1999, he was a European Union Training and Mobility of Researchers Research Fellow with the University of Perugia, Perugia, Italy, where he worked on the design and simulation of quasi-optical multipliers using the lumped-element finite-difference time-domain (FDTD) method. From 2000 to 2002, he was a Research Associate with the University of Bristol, Bristol, U.K., where he worked on hybrid electromagnetic methods for electromagnetic-compatibility problems in optical transceivers and FDTD analysis of photonic crystals. He is currently a Senior Lecturer with the Department of Electrical and Electronic Engineering, University of Bristol. He has published 25 journal papers and 76 conference proceedings (including seven invited) on fabrication, modeling, and measurement of photonic-crystal-based devices, RF-over-fiber, active integrated antennas, FDTD analysis, and monolithic microwave integrated-circuit design.